Two-photon magnetoabsorption spectroscopy in n-InSb with cw CO_2 lasers

M. W. Goodwin and D. G. Seiler
Center for Applied Quantum Electronics, North Texas State University, Denton, Texas 76203

M. H. Weiler
Department of Physics, Massachusetts Institute of Technology, Cambridge, Massachusetts 02139

(Received 22 December 1981)

High-resolution two-photon magnetoabsorption (TPMA) spectra are obtained for $\vec{e}\perp\vec{B}$ and $\vec{e}||\vec{B}$ polarizations in the Voigt geometry. The use of cw CO_2 lasers and a sensitive photoconductivity technique have allowed the observation of many new TPMA transitions. A modified Pidgeon-Brown energy-band model, along with the usual spherical two-photon selection rules, explains most of the observed transitions. The temperature dependence of the energy gap is deduced from an analysis of the TPMA spectra at various temperatures.

I. INTRODUCTION

Magneto-optical investigations of two-photon processes are particularly valuable for studying nonlinear absorption in semiconductors. The selection rules for two-photon magnetoabsorption (TPMA) allow completely different transitions to occur than for one-photon magnetoabsorption. In previous experiments of TPMA in InSb, pulsed lasers were used because it was believed that high intensities were necessary to observe two-photon transitions. However, we have recently shown that for the first time in solids, cw lasers operating at even milliwatt powers can be used in the study of TPMA if a sensitive enough detection method like photoconductivity (pc) is used.[1] Derivative TPMA spectroscopy with sampling and magnetic field modulation techniques applied to the pc signal further allows the observation of weak transitions in the TPMA pc spectra that would otherwise be unobservable.

In this paper we present comprehensive results on the TPMA spectra for both $\vec{e}\perp\vec{B}$ and $\vec{e}||\vec{B}$ in the Voigt geometry for various lattice temperatures from 1.8 to 100 K. Most of the observed transitions are adequately explained by the spherical selection rules $\Delta s=0$, $\Delta n=0,\pm 2$, and a Pidgeon-Brown model calculation for the Landau-level energies. For the first time, we determine a set of band parameters for InSb from our TPMA experiments. By observing the resonant structure at different temperatures, we determine the variation of the energy gap with lattice temperature and compare it to previous experiments and theoretical results. From measurements of the number of two-photon-produced carriers as a function of laser intensity, we estimate TPMA coefficients for some of the stronger transitions. To our knowledge this is the first time that TPMA coefficients have been calculated from magnetophotoconductivity experiments.

The first TPMA experiments in InSb were carried out by Button *et al.*[2] using a Q-switched CO_2 laser simultaneously oscillating on two lines. They observed resonant structure in the photoconductivity caused by two-photon absorption between Landau levels in the valence and conduction bands. Zawadzki, Hanamura, and Lax[3] were the first to develop a set of two-photon selection rules using a time-dependent perturbation-theory approach. Later, Weiler *et al.*[4] extended Keldysh's[5] tunneling theory to the magnetic field case to try to explain the observed[6] polarization dependence ($\vec{e}\perp\vec{B}$ and $\vec{e}||\vec{B}$). However, this theory was later found to be incorrect for two- (or even-) photon absorption and was shown to reduce to the perturbation-theory result.[7,8] Perturbation theory was again used by Bassani and Girlanda[9] to calculate explicit expressions for the two-photon transition rate in a magnetic field. TPMA experiments on InSb were continued by Nguyen and Strnad[10] and Nguyen *et al.*[11] who studied the absorption by free holes created by the two-photon processes using a Q-switched CO_2 laser pulse. Both linearly polarized light with $\vec{e}||\vec{B}$ and $\vec{e}\perp\vec{B}$ and left (σ_L) and right (σ_R) circularly polarized light were used. They compared the experimental absorption strengths of the two-photon transitions for $\vec{e}\perp\vec{B}$ ($\sigma_L,\sigma_R,\sigma_L+\sigma_R$) with a

theoretical calculation based on the perturbation-theory approach and found reasonably good agreement. However, only a small number of transitions were observed and only one-photon energy was used. Manlief and Palik[12] extended the TPMA experiments to investigate the differences between the light polarizations $\vec{e}\perp\vec{B}$ and $\vec{e}||\vec{B}$ in the Voigt configuration. The light source was a transversely excited atmospheric (TEA) CO_2 laser with an intracavity grating which allowed the photon-energy dependence of the TPMA transition to be studied. Their use of the photoconductivity technique enabled more transitions to be observed than were found by Nguyen *et al.* However, their transition assignments were somewhat ambiguous because of the uncertainty of both their measurements and the one-photon-interband Landau-energy data that was used to obtain the transition energies for their two-photon case. Nevertheless, they found several transitions in their studies which were not adequately explained by the usual spherical selection rules obtained from ordinary perturbation theory. In this paper we give transition assignments that are more unambiguous because (1) the higher resolution of our data allows more transitions to be seen, and (2) the data are compared with two-photon transition energies actually calculated from a Pidgeon-Brown model with band parameters adjusted to give a best fit.

Selection rules are extremely important for a good description of the two-photon magnetoabsorption process. The most complete summary of the two-photon selection rules for the different light polarizations (σ_L, σ_R, σ, and π) was given by Zawadzki and Wlasak, but only for the case of $\vec{B}||[001]$.[13] Extra transitions were shown to occur because of warping and inversion-asymmetry effects. In this paper we give more complete two-photon selection rules for the different light polarizations and for $\vec{B}||[111]$ and [110] directions, as well as the [001] direction.

II. EXPERIMENT

The samples of high-purity n-InSb ($\sim 9\times 10^{13}$ cm^{-3}) were mounted in the Voigt configuration with the current parallel to the magnetic field $\vec{B}$ and $\vec{B}$ parallel to [110] [100] and [111] crystallographic directions. Light from a grating-tunable cw CO_2 laser was mechanically chopped by a rotating slotted wheel to produce optical pulses of approximately 20-μsec width at a repetition rate of 1700 Hz. This minimized heating of the sample which was either immersed in liquid helium or surrounded by flowing helium gas for the higher temperature measurements. To vary the intensity of the laser we placed CaF_2 attenuators in the beam path. Beam profile measurements at the sample location showed that the beam was Gaussian with a typical $1/e$ intensity diameter of approximately 0.5 mm. A boxcar integrator was used to measure directly the photoconductive voltage, which at low powers is related to the number of two-photon-produced photocarriers. Field positions, amplitudes, and line widths can then be directly measured and studied as a function of laser intensity, lattice temperature, etc. The addition of modulation techniques significantly improves the sensitivity and resolution of photoconductivity experiments allowing a more accurate determination of the resonant field positions and resolution of weak structure.

A variation of the sampling and magnetic field modulation technique developed by Kahlert and Seiler,[14] for hot-electron quantum transport measurements is used to improve greatly the signal-to-noise ratio in photoconductivity measurements. A constant dc electrical current is applied to the sample while an ac magnetic field B_m of amplitude up to 200 G modulates the sample conductivity at a freqency of 43 Hz. The photoconductive signal produced by the laser pulse and the field modulation is amplified by a high-impedance differential amplifier, the output of which is connected to a sampling oscilloscope and lock-in amplifier combination.

In Fig. 1 we demonstrate how powerful the photoresistance-derivative technique is by comparing traces obtained with the sampling oscilloscope and lock-in amplifier combination (d^2R/dB^2, dR/dB) to that obtained with a boxcar averager (R). As can be seen, the TPMA structure in the d^2R/dB^2 trace is much sharper and more pronounced than in the R trace, making determination of magnetic field positions for the transitions not only easier but more accurate. The field positions of the resonant structure are not changed by the modulation technique. In addition, and most importantly, the second-derivative technique is able to resolve very weak structure that is marginally or not at all observable in the R trace (note the dotted lines). This is one reason we are able to observe more TPMA transitions than have previously been reported. The use of stable cw lasers also reduces the pulse-to-pulse amplitude variation usually present from pulsed lasers. The resulting enhanced

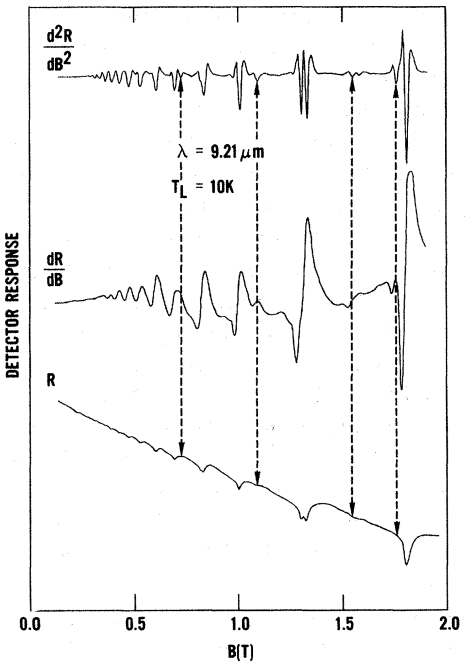

FIG. 1. Comparison of TPMA data using our high-resolution technique and that obtained with a boxcar averager. The d^2R/dB^2 and dR/dB curves are the second and first derivative of the magnetophotoresistance R with respect to magnetic field B using the sampling and magnetic-field modulation system. R is the magnetophotoresistance of the sample obtained with a boxcar averager commonly used on other experiments. The dashed lines point to weak transitions in d^2R/dB^2 not found in the R traces. ($B_m = 200$ G.)

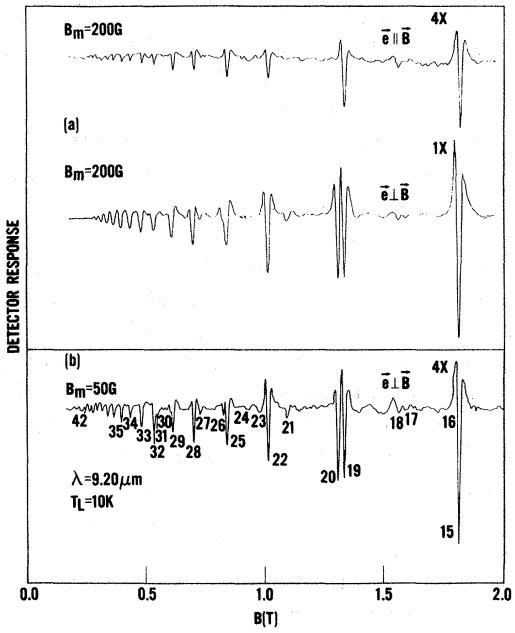

FIG. 2. (a) Comparison of TPMA structure for $\vec{e}\|\vec{B}$ and $\vec{e}\perp\vec{B}$ with $B_m = 200$ G. (b) Increased resolution of structure for $\vec{e}\perp\vec{B}$ using $B_m = 50$ G.

signal-to-noise ratio thus allows more TPMA transitions to be seen at low fields where the TPMA transition strength is weak.

III. RESULTS

A. Transition energies

An interesting aspect of two-photon magnetoabsorption and one that has been the subject of much controversy is the effect of different polarizations of the light on the TPMA spectra. Such effects are a consequence of the selection rules, which are different for different polarizations. In Fig. 2(a) the resonant structure caused by the polarizations $\vec{e}\perp\vec{B}$ and $\vec{e}\|\vec{B}$ in the Voigt configuration is shown. The structure is labeled with numbers corresponding to distinct sets of transitions. Two major observations about these transitions are apparent: (1) those for $\vec{e}\|\vec{B}$ are much weaker than those for $\vec{e}\perp\vec{B}$ and (2) for $\vec{e}\perp\vec{B}$, more complex structure is seen. Previous studies[10,12] of TPMA with pulsed lasers also showed this. The complexity of the $\vec{e}\perp\vec{B}$ structure is much more evident in Fig. 2(b) where a lower modulation field $B_m \simeq 50$ G results in small resonant amplitudes but allows resolution of fine structure down to very low magnetic fields. For example, we have complete resolution of a "double nature" to lines 19,20,22,23,25–32, while evidence for doublets from the line shape can still be seen in lines 33–35. Previous TPMA experiments did not have the resolution to detect this nature of the actual TPMA structure.

In Table I we have listed the two-photon magnetoabsorption selection rules derived from the usual spherical approximation and additional selection rules which are allowed because of warping and inversion-asymmetry effects. We have included the selection rules for the case of $\vec{B}\|[111]$ and $\vec{B}\|[110]$ by extending the one-photon selection rules of Weiler *et al.*[15] to the two-photon absorption case. Transitions within the a and b set of solutions are denoted by $\Delta s = 0$, while $\Delta s = -1$ denotes transitions from a to b and $\Delta s = +1$, b to a. Also given is the corresponding change in Landau-level number Δn from the initial valence-band state to the final conduction-band state using the unrenumbered valence-band-state notation. In

TABLE I. Selection rules for two-photon transitions in zinc-blende semiconductors, for a magnetic field $\vec{B}||[001]$, [110], and [111] crystal axes, both allowed (A) and induced by warping (W) and inversion asymmetry (I).

		$\vec{B}\|\|[001]$						$\vec{B}\|\|[110]$				$\vec{B}\|\|[111]$			
		A		W		I		W		I		W		I	
Polarization		Δs	Δn	Δs	Δn	Δs	Δn	Δs	Δn	Δs	Δn	Δs	Δn	Δs	Δn
	σ_L	0	+2	0	−2, +6	−1	+1, +5	0	0, 2 +4, +6	0	±1, +3, +5	−1	0, +6	0	−1+5
														−1	+3
						+1	−1, +3					+1	−2, +4	+1	+1
$\vec{E}\perp\vec{B}$	σ_R	0	−2	0	+2, −6	−1	+1, −3	0	0, +2 −4, −6	0	±1,	−1	+2, −4	0	+1, −5
														−1	−1
						+1	−1, −5					+1	0, −6	+1	−3
	σ	0	0	0	±4	−1	±1, ±3	0	±2, ±4	0	±1, ±3	−1	−2, +4	0	±3
														−1	+1
						+1	±1, ±3					+1	+2, −4	+1	−1
$\vec{E}\|\|\vec{B}$	π	0	0	0	±4	−1	±1, ±3	0	±2, ±4	0	±1, ±3	−1	−2, +4	0	±3
														−1	+1
						+1	±1, ±3					+1	+2, −4	+1	−1

agreement with the data (1) the spherical approximation rules predict more transitions for $\vec{e}\perp\vec{B}$ than for $\vec{e}||\vec{B}$ and (2) some of the transitions should be the same for both light polarizations (i.e., $\Delta n=0, \Delta s=0$).

Quantitative results of transition energies (twice the photon energy) versus resonant magnetic field positions are shown in Fig. 3 for both (a) $\vec{e}\perp\vec{B}$ and (b) $\vec{e}||\vec{B}$ along with theoretically calculated results with $\vec{B}||[110]$. There are many more transitions plotted than have been found from the earlier studies using pulsed lasers.[2,6,10–12] We have added several weaker transitions to the $\vec{e}\perp\vec{B}$ set reported earlier by us.[1] In Table II, we give the theoretical assignments of the intial and final states to the experimentally observed two-photon transitions. The experimental positions of our two-photon structure are in good agreement with those published in Refs. 10–12. In addition, it is interesting to note that our identification of the transitions 4, 5, 7, 9, 10, 12, 15, and 20 is the same as that in Refs. 10 and 11, whereas the identification in Ref. 12 is the same for only transitions 4, 7, 10, 11, and 15. The Landau levels were calculated from an 8×8 Pidgeon-Brown model which includes only the warping terms in the diagonal part of the Hamiltonian and no inversion asymmetry terms.[15,16] Transitions involved in magnetoabsorption experiments are usually considered as being to exciton levels rather than being between the Landau levels. However, there is at present no adequate exciton theory for TPMA in semiconductors with complex coupled energy bands. In our earlier approach[1] we reduced the calculated interband transition energy by an approximate exciton ground-state binding energy. This is the standard exciton correction used in one-photon spectroscopy. Here we adopt the approach of not correcting for exciton effects and of treating the Landau-level theory as accurately as possible in calculating transition energies. We then look for differences between the calculated and observed energies for the lowest transitions where exciton effects should be most important. The theortically calculated *solid lines* shown in Fig. 3 result from using only the spherical selection rules given in Table I. It appears that most of the experimental data can be adequately described (but with a new set of band parameters) with these rules without using exciton corrections even for the low-energy high-field transitions. A good fit of these theoretical transitions to the data results from using the following band parameters: $E_g=235.2$ meV, $E_p=23.0$ eV, $\Delta=0.803$ eV, $\gamma_1=3.0$, $\gamma_2=-0.2$, $\gamma_3=1.0$, $\kappa=-1.2$, $q=0.55$, $F=-0.5$, and $N_1=-0.4$. No attempt was made to determine a value of Δ from our two-photon data. Instead we have used the stress-modulated magnetoreflectance results of $\Delta=0.803\pm0.005$ eV obtained by Aggarwal.[17] Our results for the rest of the band parameters are compared in Table III

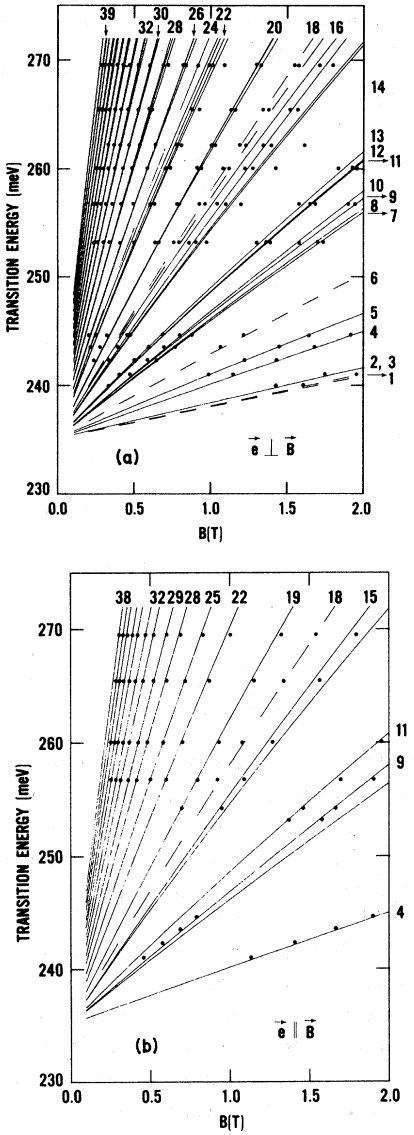

FIG. 3. (a) Fan chart of TPMA transition energies ($\vec{e}\perp\vec{B}||[110]$). Solid lines represent theoretical calculations with selection rules $\Delta s=0$, $\Delta n=0,\pm 2$. Dotted lines used other selection rules explained in the text. Dots are the data. (b) Fan chart for $\vec{e}||\vec{B}$.

with previously published one-photon results of Grisar *et al.*,[18] Ranvaud *et al.*,[19] Weiler,[20] Pidgeon and Brown,[16] and Pidgeon and Groves.[21] We have used this same set of parameters in also fitting intra-conduction-band (combined resonance, cyclotron resonance, and LO phonon-assisted resonances)[22] and intra-valence-band (both bound and free-hole transitions)[23] data. An excellent fit in both cases is achieved.

Additional weaker structure labeled (1,3), (6), (17,18), and (24) in Fig. 3 appears not to be explainable by the spherical selection rules. We find that lines 1,3 may be explained by spin-flip transitions $b^-(1)\rightarrow a^c(0)$ ($\Delta s=+1$, $\Delta n=-1$) and $b^+(-1)\rightarrow a^c(0)$ ($\Delta s=+1$, $\Delta n=+1$). These are shown by the dashed lines in Fig. 3. According to Table I these transitions are allowed because of inversion-asymmetry effects but only for $\vec{B}||[100]$ or [111]. Transition 6 was also observed by Manlief and Palik for $\vec{B}||[100]$ at higher magnetic fields and higher photon energies and was identified with an $a^+(0)\rightarrow b^c(0)$ ($\Delta s=-1$, $\Delta n=0$) transition. Using this transition we calculate an additional line passing exactly through our data points in set 6 (as shown by the dashed line) confirming this identification. Transitions in set 17, 18, and 24 have not been previously reported. They are very weak resonances which can only be observed using the modulation technique. Our calculations support the identification for an $a^+(2)\rightarrow b^c(0)$ transition with $\Delta s=-1$ and $\Delta n=-2$ for 17 and $a^+(1)\rightarrow b^c(1)$ and $a^+(2)\rightarrow b^c(2)$ transitions with $\Delta s=-1$ and $\Delta n=0$ for 18 and 24, respectively. According to Table I $\Delta s=-1$, $\Delta n=0$ transitions can occur for $\vec{B}||[111]$ because of warping effects. However, these transitions are also present for $\vec{B}||[100]$ and [110] is not presently understood.

B. Effect of lattice temperature

TPMA experiments provide an accurate means of determining the variation of the fundamental energy gap E_g with lattice temperature T_L. Figure 4 shows how the TPMA spectra at $\lambda=9.33$ μm is affected by increasing T_L for $T_L\leq 100$ K. The shift in magnetic field positions of the resonant structure is quite noticeable for $T_L\geq 30$ K and is directly related to the decrease in energy gap with increasing temperature. At each value of T_L, fan charts of transition energies versus magnetic field were determined and analyzed assuming that all parameters except E_g were constant. The results are shown in Fig. 5 where a comparison with theoretical calculations of Tsay *et al.*[24] and Camassel and Auvergne[25] is also given. These theoretical results were normalized to our experimental band gap of 235.2 meV at $T_L\leq 10$ K. Also shown are the experimental results of Roberts and Quarrington[26] and Auvergne *et al.*[27] There is good agreement between our data and the results of Cammassel and Auvergne who directly calculated the temperature dependence using a pseudopotential approach. With increasing T_L one increases both the lattice constant and the electron-phonon

TABLE II. Theoretical two-photon transition assignments for each distinct experimentally observed series of resonant structure in the photoconductivity for $\vec{e}\perp\vec{B}$ polarization in the Voigt geometry. The * marks indicate those transitions which can only be explained by the nonspherical or extra transitions.

Experimental transition no.	Theoretical assignment	Experimental transition no.	Theoretical assignment
*1,3	$a^-(1)\,a^c(0)$	20	$b^+(0)\,b^c(2)$
	$a^+(-1)\,a^c(0)$	21	$a^+(3)\,a^c(1)$
	$b^-(2)\,a^c(0)$	22	$a^-(6)\,a^c(4)$
	$b^-(1)\,a^c(0)$		$a^+(2)\,a^c(2)$
	$b^+(-1)\,a^c(0)$	23	$b^-(6)\,b^c(4)$
2	$a^-(2)\,a^c(0)$	*24	$a^+(2)\,b^c(2)$
4	$a^+(0)\,a^c(0)$	25	$a^-(7)\,a^c(5)$
5	$b^-(2)\,b^c(0)$		$b^+(2)\,b^c(2)$
*6	$a^+(0)\,b^c(0)$	26	$b^+(1)\,b^c(3)$
7	$a^+(-1)\,a^c(1)$	27	$a^+(4)\,a^c(2)$
8	$a^-(1)\,a^c(1)$	28	$a^-(8)\,a^c(6)$
9	$b^+(0)\,b^c(0)$		$a^+(3)\,a^c(3)$
10	$a^-(3)\,a^c(1)$	29	$a^-(9)\,a^c(7)$
11	$b^-(1)\,b^c(1)$		$b^+(3)\,b^c(3)$
12	$b^+(-1)\,b^c(1)$	30	$b^+(2)\,b^c(4)$
13	$b^-(3)\,b^c(1)$	31	$a^+(5)\,a^c(3)$
14	$a^+(2)\,a^c(0)$	32	$a^-(10)\,a^c(8)$
15	$a^-(4)\,a^c(2)$		$a^+(4)\,a^c(4)$
	$a^+(1)\,a^c(1)$	33	$b^+(3)\,b^c(5)$
16	$b^-(4)\,b^c(2)$		$a^-(11)\,a^c(9)$
*17	$a^+(2)\,b^c(0)$		$b^+(4)\,b^c(4)$
	$a^-(4)\,b^c(2)$	34	$a^+(6)\,a^c(4)$
*18	$a^+(1)\,b^c(1)$		$a^-(12)\,a^c(10)$
	$a^+(0)\,b^c(2)$		$a^+(5)\,a^c(5)$
	$b^+(2)\,b^c(0)$	35	$b^+(4)\,b^c(6)$
19	$a^-(5)\,a^c(3)$		$a^-(13)\,a^c(11)$
	$b^+(1)\,b^c(1)$		$b^+(5)\,b^c(5)$

TABLE III. Energy-band parameter sets for InSb from various experiments.

Parameter	Grisar *et al.* (Ref. 18)	Ranvaud *et al.* (Ref. 19)	Weiler (Ref. 20)	Pidgeon and Brown (Ref. 16)	Pidgeon and Groves (Ref. 21)	This paper
E_g (eV)	0.2355	0.235	0.2329	0.2355 ±0.0005	0.2366	0.2352
E_p (eV)	21.6	26.1	23.5±0.5	21.9	21.2	23.0
γ_1	0.5	3.1	3.4	1.5	3.6	3.0
γ_2	−1.0	−0.4	−0.3	−1.2	−0.5	−0.2
γ_3	0.1	0.7	0.9	−0.1	0.7	1.0
$\gamma_2-\gamma_3$	−1.1	−1.1	−1.2	−1.1	−1.2	−1.2
κ	−1.4	−1.5	−1.2	−2.1	−1.47	−1.2
q	0	0.39	0	0	0.39	0.55
N_1	0	0	−0.3	0	0	−0.4
F	0	0	−1.0	0	0	−0.5

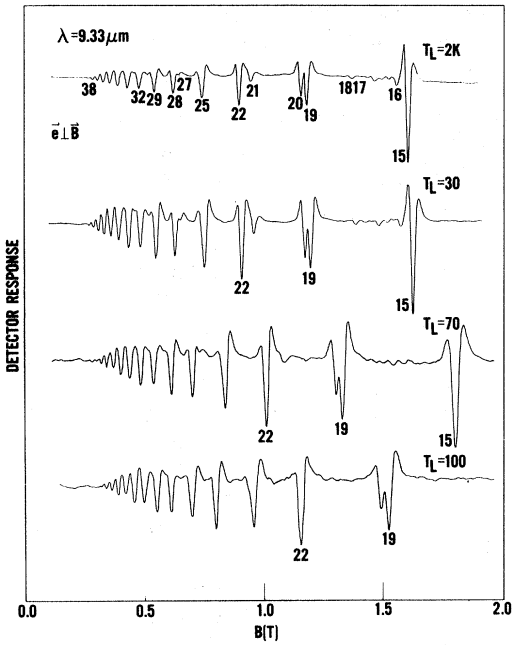

FIG. 4. Temperature dependence of TPMA structure for $\lambda=9.33\ \mu$m.

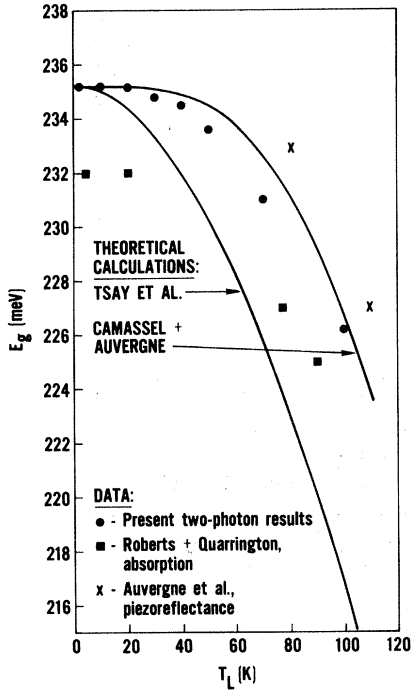

FIG. 5. Plot of energy gap vs temperature from our TPMA measurements and other results. The lines are theoretical calculations of Tsay *et al* (Ref. 24) and of Cammassel and Auvergne (Ref. 25) normalized to $E_g=235.2$ meV.

interaction. Their contributions to the gap change are of opposite sign leading to only slight decreases in band gap for $T_L \lesssim 25$ K. The gap at 77 K is thus approximately 230 meV.

C. Intensity dependence

Figure 6 shows the TPMA structure for the "low-intensity" case using a cw CO_2 laser and for that obtained using a rotating mirror Q-switched CO_2 laser operating at 200 Hz with a pulsewidth of full width at half maximum of 100 nsec. There is good agreement between the observed structures. Since no additional structure is observed in the rotating mirror case, one concludes that this is additional confirmation of the correct identification of the cw laser-induced structure as indeed arising from TPMA effects. It is also apparent that in the cw case we have really reached the "high-intensity" limit where TPMA effects can be observed at rather low powers.

Two-phonon absorption is a nonlinear process which has a nonlinear dependence on the incident intensity. The two-photon absorption coefficient K_2, which is a parameter of the semiconductor and

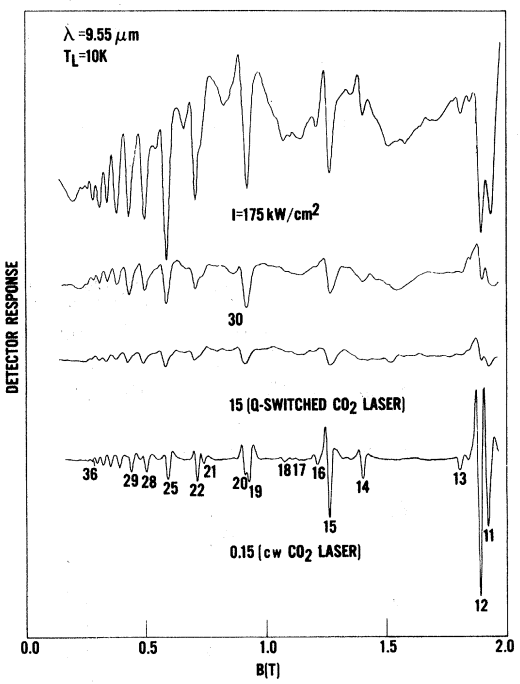

FIG. 6. TPMA structure obtained with a Q-switched CO_2 laser (top 3 traces) and with a cw CO_2 laser for $\lambda=9.55\ \mu$m.

describes the rate of two-photon-produced free carriers, has been the subject of intense experimental studies.[28–34] However, these results are not consistent. For this reason we have determined two-photon absorption coefficients for some of the stronger transitions in our pc data.

The standard approach for describing the rate of two-photon-generated carriers is to assume that an electron in the valence band is excited into the conduction band via two-photon absorption and then decays by the bimolecular process of radiative recombination. A suitable rate equation can then be written

$$\frac{dn}{dt}=\frac{K_2}{2\hbar\omega}I^2-rn(n+n_0)\,, \tag{1}$$

where n is the photon-created carrier density, K_2 the two-photon magnetoabsorption coefficient, $\hbar\omega$ the photon energy, I the incident intensity, r the recombination rate, and n_0 the equilibrium carrier density without light. The time duration of our optical pulses is suffficiently long enough (20 μsec) that a steady state occurs at the time of our measurements, usually 10 μsec after the beginning of the pulse. For steady state $dn/dt=0$, simplifying Eq. (1) tremendously. For the low laser intensities (<200 W/cm^2) of our study the photon-created carrier density n is small (i.e., $n<<n_0$). With these assumptions Eq. (1) is reduced to the following:

$$n=\frac{K_2}{2\hbar\omega r n_0}I^2\,, \tag{2}$$

which shows that the number of free carriers produced by TPMA is proportional to I^2. Also considered in many TPMA experiments is the depletion of the laser intensity as it propagates through the crystal. For our sample thickness of approximately 100 micrometers we estimate that the change in intensity of the beam from the front to the back surface is roughly 0.01% for the highest intensities reported here. We therefore neglect the change in intensity of the laser beam and assume a uniform constant Gaussian optical flux throughout the sample.

In Fig. 7 we have plotted n vs I^2 for five different laser intensities for the strong transition labeled 12 ($\vec{e}\perp\vec{B}$) of Fig. 3. Assuming a negligible change in mobility, the photocreated carrier densities were determined from the amplitude of the resonant resistance structure obtained with a boxcar averager (an example of the structure for a different wavelength is trace R of Fig. 1). Thus n is seen to vary approximately as I^2 in agreement with Eq. (2). At higher intensities the amplitude of the resonant structure is observed to depart significantly from a square-law behavior because of hot-electron and free-hole absorption effects. Also plotted in Fig. 7 is a fit of Eq. (2) to the data using K_2 as an adjustable parameter. The value of the other parameters are $\hbar\omega=128.14$ meV, $r=1\times10^{-9}$ cm^3/sec,[35] $n_0=9\times10^{13}$ cm^{-3}, giving a value of K_2 of 5.6 cm/MW. For the same transition above at a slightly higher magnitude field (1.92 T) and higher photon energy (129.8 meV) Nguyen *et al.*[10] obtained a value for K_2 of 16.6 cm/MW. Their somewhat larger value of K_2 is partly due to that fact that a higher magnetic field will increase the magnitude of K_2 for a particular transition. However, it must be pointed out that our K_2 is sensitive to a proper choice of the recombination rate r. Another problem that arises when trying to extract information about an individual transition is that a minimum in the structure may actually be a combination of two or more transitions. The large number of transitions (theory and experiment) evident in Fig. 3 certainly seem to indicate this. Therefore, K_2 was calculated and measured only for a strong transition which was minimally influenced by a presence of other closely-spaced weak transitions.

IV. CONCLUSIONS

High-resolution TPMA spectra in InSb for $\vec{e}\perp\vec{B}$ and $\vec{e}\|\vec{B}$ polarizations in the Voigt geometry have been investigated using cw CO_2 lasers. A highly

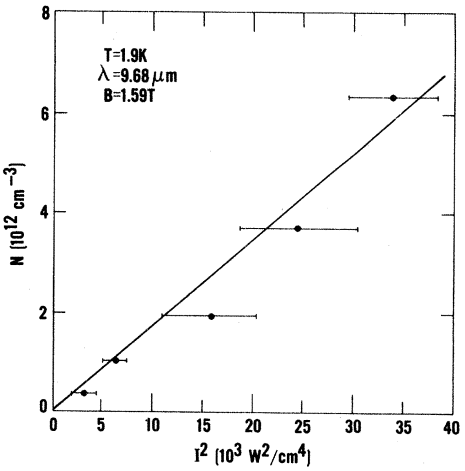

FIG. 7. Two-photon-produced free-carrier density as a function of intensity for transition 12. The line represents the variation of Eq. (2) with $K_2=5.7$ cm/MW.

sensitive photoconductivity technique in conjuction with a stable cw laser have allowed the observation of many new TPMA transitions. Previous TPMA experiments have not been able to show how complicated the two-photon spectra really is. Many of the previously observed transitions are shown to be combinations of two or more transitions. A minimum of 42 distinct transitions are observed and identified for $\vec{e}\perp\vec{B}$, most of which can be explained by the usual spherical two-photon selection rules $\Delta n=0,\pm 2$, $\Delta s=0$. For $\vec{e}\|\vec{B}$ the structure is less complicated and can be explained by the spherical rule $\Delta n=0$, $\Delta s=0$. A modified Pidgeon-Brown energy-band model, along with these spherical selection rules explain most of the observed transitions using the following set of band parameters: $E_g=235.2$ meV, $E_p=23.0$ eV, $\Delta=0.803$ eV, $\gamma_1=3.0$, $\gamma_2=-0.2$, $\gamma_3=1.0$, $\kappa=-1.2$, $F=-0.5$, $q=0.55$, and $N_1=-0.4$. Additional weaker TPMA transitions appear to result from warping and inversion-asymmetry effects. The variation of the fundamental energy gap with lattice temperature is deduced from an analysis of the temperature-dependent TPMA spectra. Our results give a gap of ~ 230 meV at 77 K and compare favorably with the pseudopotential calculations of Camassel and Auvergne. At low intensities the number of photoexcited electrons varies approximately as the square of the incident intensity, as predicted by a simple rate equation model.

Note added in proof. Band-gap renormalization caused by many-body effects of the laser-created electron-hole plasma would be expected to decrease the energy gap. The amount of decrease depends upon the laser intensity which also controls the number of electron-hole pairs. However, the magnetic field positions of the resonances shown in Fig. 6 do not appear to shift even at the high intensities from the Q-switched laser. Thus the band-gap change with these high intensities must be much less than 1 meV. Recently Koch *et al.*[36] calculated the change in band gap as a function of electron-hole pair density for InSb. Since the number of created electron-hole pairs at the large intensities is estimated to be at least $10^{14}-10^{15}$ cm^{-3} their results indicate a much larger band-gap renormalization effect when we observe (at 10^{15} cm^{-3} their calculated decrease is approximately 2.5 meV).

[1]D. G. Seiler, M. W. Goodwin, and M. H. Weiler, Phys. Rev. B 23, 6806 (1981).

[2]K. J. Button, B. Lax, M. H. Weiler, and M. Reine, Phys. Rev. Lett. 17, 1055 (1966).

[3]W. Zawadzki, F. Hanamuara, and B. Lax, Bull. Amer. Phys. Soc. 12, 100 (1967).

[4]M. H. Weiler, M. Reine, and B. Lax, Phys. Rev. 171, 949 (1968).

[5]L. V. Keldysh, Zh. Eksp. Teor. Fiz. 47, 1945 (1964) [Sov. Phys.—JETP 20, 1307 (1965)].

[6]M. H. Weiler, R. Bierig, and B. Lax, Phys. Rev. 184, 709 (1969).

[7]M. H. Weiler, Phys. Rev. B 7, 5403 (1973).

[8]Y. N. Bychkov and A. M. Dykhne, Zh. Eksp. Teor. Fiz. 58, 1734 (1970) [Sov. Phys.—JETP 31, 928 (1970)].

[9]F. Bassani and R. Girlanda, Opt. Commun. 1, 359 (1970).

[10]V. T. Nguyen and A. R. Strnad, Opt. Commun. 3, 25 (1971).

[11]V. T. Nguyen, A. R. Strnad, and Y. Yafet, Phys. Rev. Lett. 26, 1170 (1971).

[12]S. K. Manlief and D. E. Palik, Solid State Commun. 12, 1071 (1973).

[13]W. Zawadzki and J. Wlasak, J. Phys. C 9, L663 (1976).

[14]H. Kahlert and D. G. Seiler, Rev. Sci. Instrum. 48, 1017 (1977).

[15]M. Weiler, R. L. Aggarwal, and B. Lax, Phys. Rev. B 17, 3269 (1978).

[16]C. R. Pidgeon and R. N. Brown, Phys. Rev. 146, 575 (1966).

[17]R. L. Aggarwal, in *Semiconductors and Semimetals,* edited by R. K. Willardson and A. C. Beer (Academic, New York, 1972), Vol. 9, p. 151.

[18]R. Grisar, H. Wachernig, G. Bauer, J. Wlask, J. Kowalski, and W. Zawadzki, Phys. Rev. B 18, 4355 (1978).

[19]R. Ranvaud, H. -R. Trebin, U. Rossler, and F. H. Pollak, Phys. Rev. B 20, 701 (1979).

[20]M. H. Weiler, J. Magn. Magn. Mater. 11, 131 (1979).

[21]C. R. Pidgeon and S. H. Groves, Phys. Rev. 186, 824 (1969).

[22]M. W. Goodwin and D. G. Seiler (unpublished).

[23]C. L. Littler, D. G. Seiler, R. Kaplan, and R. J. Wagner (unpublished).

[24]Y. F. Tsay, B. Gong, S. S. Mitra, and J. F. Vetelino, Phys. Rev. B 6, 2330 (1972).

[25]J. Camassel and D. Auvergne, Phys. Rev. B 12, 3258 (1975).

[26]V. Roberts and J. E. Quarrington, J. Electron. 1, 152 (1955).

[27]D. Auvergne, J. Camassel, H. Mathieu, and M. Cardo-

na, Phys. Rev. B 9, 5168 (1974).
[28]A. F. Gibson, M. J. Kent, and M. F. Kimmitt, Brit. J. Appl. Phys. 1, 149 (1968).
[29]A. M. Danishevskii, A. A. Patrin, S. M. Ryvkin, and J. D. Yaroshetskii, Zh. Eksp. Teor. Fiz. 56, 1459 (1969) [Sov. Phys.—JETP 29, 781 (1969)].
[30]J. M. Doviak, A. F. Gibson, M. F. Kimmitt, and A. C. Walker, J. Phys. C 6, 593 (1973).
[31]H. J. Fossum and D. B. Chang, Phys. Rev. B 8, 2842 (1973).
[32]C. C. Lee and H. Y. Fan, Phys. Rev. B 9, 3502 (1974).
[33]A. F. Gibson, C. B. Hatch, P. N. D. Maggs, D. R. Tilley, and A. C. Walker, J. Phys. C 9, 3529 (1976).
[34]A. Miller, A. Johnston, J. Dempsey, J. Smith, C. R. Pidgeon, and G. D. Holah, J. Phys. C 12, 4839 (1979).
[35]H. J. Fossum and B. Ancker-Johnson, Phys. Rev. B 8, 2850 (1973).
[36]S. W. Koch, S. Schmitt-Rink, and H. Haug, Phys. Status Solidi B 106, 135 (1981).